CrossMark

Characterizing the hydraulic properties of paper coating layer using FIB-SEM tomography and 3D pore-scale modeling

H. Aslannejad[a,*], S.M. Hassanizadeh[a], A. Raoof[a], D.A.M de Winter[a], N. Tomozeiu[b], M.Th. van Genuchten[a,c]

[a] *Multiscale porous media lab., Department of Earth Sciences, Utrecht University, Utrecht, The Netherlands*
[b] *R & D Department, Océ Technologies B.V., Venlo, The Netherlands*
[c] *Department of Mechanical Engineering, Federal University of Rio de Janeiro, Rio de Janeiro, Brazil*

ARTICLE INFO

ABSTRACT

Paper used in the printing industry generally contains a relatively thin porous coating covering a thicker fibrous base layer. The three-dimensional pore structure of coatings has a major effect on fluid flow patterns inside the paper medium. Understanding and quantifying the flow properties of thin coating layers is hence crucial. Pore spaces within the coating have an average size of about 180 nm. We used scanning electron microscopy combined with focused ion beam (FIB-SEM) to visualize the nano-scale pore structure of the paper coating layer. Post-processing of the FIB-SEM images allowed us to reconstruct the three-dimensional pore space of the coating. The 3D FIB-SEM images were analyzed in detail to obtain pore size distribution and porosity value. The permeability was estimated using the GeoDict software, based on solutions of the Stokes equation. By determining the porosity and permeability of increasingly larger domain sizes, we estimated the size of a representative elementary volume (REV) for the coating layer to be 60 μm^3, which is well within the volume analyzed using FIB-SEM. The estimated porosity and permeability of the REV domain were 0.34 and 0.09 mDarcy, respectively. Using the pore morphology method, capillary pressure-saturation (P_c-S) and relative permeability curves of the REV domain could be constructed next. The P_c-S curves showed that the coating had a high air entry suction, which is very favorable for printing in that ink will invade the coating as soon as it is applied to the coating. Our results are essential for macroscale modelling of ink penetration into a coating layer during inkjet printing. Macroscopic models can be valuable tools for optimization of the penetration depth and the spreading of ink on and within paper substrates.

1. Introduction

During inkjet printing, once an ink droplet reaches the paper surface, spreading and evaporation processes determine overall ink penetration. The dynamics of these processes affect the final print quality. In order to optimize ink penetration during inkjet printing, paper is often coated with a layer of ultra-fine mineral particles, usually composed of kaolin or calcium carbonate and bound together with an adhesive. Surface-modified calcium carbonate and clays, colloidal-precipitated calcium carbonate, alumina silicate, and zeolite are considered to be among the most promising pigments (Malla and Devisetti, 2005; Vikman and Vuorinen, 2004). The extent of ink penetration depends on the structure of this coating as well as on the fluid properties of the employed ink (Heard et al., 2004).

The porosity and pore size distribution of a coating layer determines the extent, speed, and final distribution of the injected ink.

Fig. 1. shows an overview of the processes that occur during inkjet printing (Kettle et al., 2010). The specified times indicate the approximate moment at which various phenomena are expected to start. The forces that cause lateral spreading of a droplet on the paper surface compete with the capillary suction of liquid into the paper (Girard et al., 2006). Capillarity is the dominant force drawing ink into the pore structure. Micro capillary penetration starts typically within 0.1 ms after the droplet arrives (Ridgway and Gane, 2002; Desie et al., 2004).

Several studies have been conducted to explore the performance of ink in different papers. Dalton et al., (2002) used secondary ion mass spectrometry and X-ray photoelectron spectroscopy (XPS) to determine the final distribution of ink a cross section of paper samples. Alam et al. (2009) used computational fluid dynamics simulations in order to calculate the permeability of three packing structures representing the coating layer of paper. Calculated permeability values were within one order of magnitude of reported experimental equivalents. Matilainen
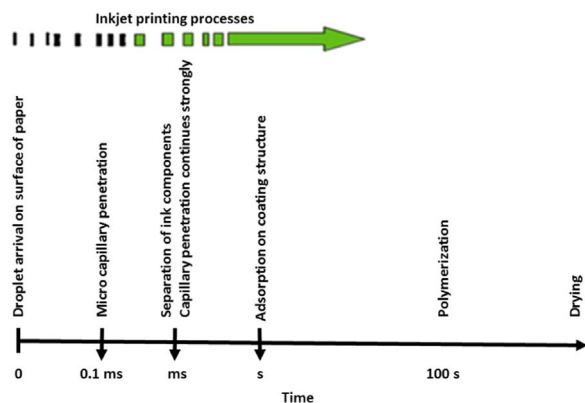
Fig. 1. Overview of processes during inkjet printing (adopted from Kettle et al., 2010).

et al., (2012) studied the spreading and penetration of bio-based ink, which contained laccase enzyme and its substrate ABTS, on three different coated printing papers. Optical and confocal microscopy techniques were used, together with a tape laminating method (Matilainen et al., 2012). The pore size distribution of the printing substrate was further explored using mercury porosimetry. Pore sizes were found to be 1–5 μm for the base layer, and 0.05–0.5 μm for the coating pores.

Lamminmäki et al., (2012) studied the coupled effects of pore structure and swelling of the binder of a coating layer on ink imbibition in terms of its penetration and spreading. The coating structure was studied with respect to its absorption behavior for polar and non-polar liquids. The measurements were performed on compressed tablets (having thicknesses of about 200 μm) containing polyvinyl alcohol (PVOH) or styrene acrylic latex (SA) as the binder. Results indicated that small pores play a dominant role in the ink imbibition process during the first two seconds. Simultaneously, water diffusion into the hydrophilic PVOH binder caused its swelling. This swelling reduced the diameters of the remaining pores, thus decreasing capillary flow. In contrast, the SA latex binder did not absorb water, which hence indicates capillary absorption was the dominant process.

Short-time processes during the early stages of ink penetration cannot be described using equilibrium fluid flow simulation methods. The liquid advance in a porous structure is usually simulated using some approximate method (e.g., (Lamminmäki et al., 2012). A well-known method is based on the Lucas–Washburn equation, which assumes that the coating consists of a collection of vertical capillary tubes. The method was improved later by Schoelkopf et al. (2002) and Ridgway and Gane (2002), who employed the Bosanquet equation (Bosanquet, 1923) to show the role of pore size and viscous drag (Ridgway et al., 2002).

The spreading and penetration of ink is generally very much affected by such paper bulk properties as porosity, permeability, thickness, moisture content, temperature, and layer structure. Gane et al. (2009) showed that standard ground calcium carbonate coatings, because of their relatively broad particle size distributions and low permeability, produce slower initial rates of adsorption of ink than more refined coating having a narrower pore size distribution and higher permeability. They found that coatings with a higher specific surface area and permeability have a faster initial moisture uptake.

The aim of this work is to obtain the detailed pore structure of a coating layer at a very high resolution, and from this its hydraulic properties using a pore-scale computational method. We first introduce a visualization method of extracting the 3D structure of the layer by using FIB-SEM imaging. The approach allowed a resolution of up to three nanometers. The method involved many cycles of removing a very thin cross-sectional layer by ion beam, and imaging by electron microscopy. Image analysis was used to obtain pore morphological information about the coating layer. Finally, using the pore morphology method, pore-scale simulations were carried out to estimate the effective hydraulic properties of the coating. Such estimates are required for continuum scale-models of ink movement in the coating layer.

2. Material and methods

2.1. Paper sample

The paper samples used in this study (i.e., Sappi Magno Gloss paper) were made of a fibrous layer covered on both sides with coating material. The total thickness of the samples was 83 μm, with a basis weight of 115 g/m² and a porosity of 0.34. The coatings, which had a thickness of 12.8 μm on each side of the paper, consisted mostly of CaCO$_3$ along with a small amount of binder. All samples were kept under room conditions (21 °C and relative humidity of 88%). A typical image of the surface and a vertical cross section of the coating are shown in Fig. 2.

2.2. FIB-SEM imaging

Samples for imaging were prepared by attaching a small piece (1 cm²) of coated paper to a standard aluminum SEM stub with a
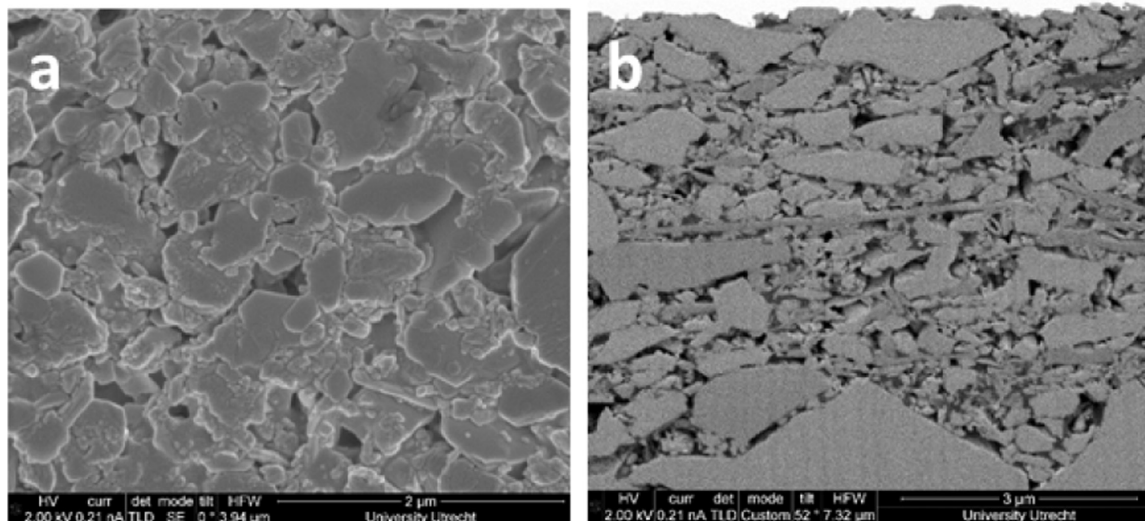

Fig. 2. Surface (a) and cross-sectional (b) views of the paper coating.
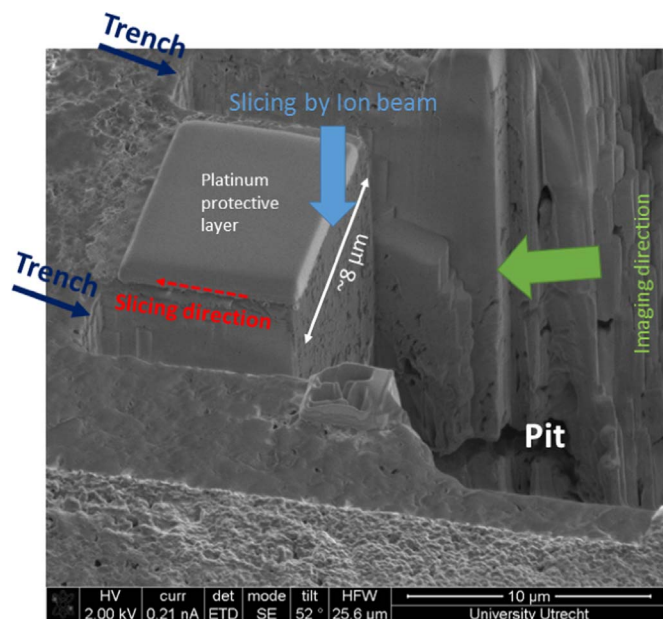
Fig. 3. An image of the coating layer under FIB-SEM tomography, showing the pit and two trenches made by the ion beam.

Fig. 4. Reconstructed FIB-SEM results showing (a) one layer of the scanned stack, (b) volume rendering of the entire scanned domain, (c) the segmented domain, and (d) labeled pores using the "Label analyzing" module.

conductive carbon sticker. The paper was sputter coated with approximately 5 nm of platinum (HQ280; Cressington Scientific Instruments Ltd, Watford, UK). The samples were placed in the vacuum chamber of a Nova Nanolab 600 focused ion beam scanning electron microscope (FIB-SEM) (FEI Company, Eindhoven, Netherlands). SEM imaging conditions were kept low to prevent potential damage of the layer by the beam. Typical imaging conditions were 2 kV and 0.21 nA. The FIB acceleration voltage was 30 kV for all processes (e.g., deposition, rough cutting, polishing); the current density was varied according to the required process.

Standard FIB-SEM tomography preparation procedures were used (Karwacki et al., 2011). An additional layer of Platinum (about 100 nm) was deposited over the area of interest to prevent damage from the FIB and to improve the finish (smoothness) of cross sections. Also, a very thin layer of platinum was deposited over a small square to the left of the area of interest, to be used as a fiducial marker for aligning both the FIB and the SEM during the FIB-SEM tomography process. Two trenches were subsequently milled alongside the area of interest (see Fig. 3) to create sufficient space for redepositing material that was removed by the FIB during tomography. A large pit (10 μm in each direction) was milled in front of the region of interest, to allow the SEM to view consecutive vertical cross sections (Fig. 3). In order to smoothen the first vertical cross section, the pit was polished with a moderate FIB current. After imaging the first cross section, FIB with a current of 0.3 nA was used to remove a 25 nm thick vertical slice and thus to expose the next cross section for electron microscopy.

The tomography measurements were carried out with the SEM recording images at 2 kV and 0.21 nA in BSE mode, with the immersion lens switched on. The scan resolution was 2048×1768 and the pixel width 3.5 nm. The dwell time was 4 μs, and the line integration two times, resulting in a frame time of approximately 35 s. A total of 678 cross sections were recorded.

2.3. Three-dimension tomography data analysis

We used Avizo Fire software 9.0 (FEI, Oregon, US) for the 3D tomography data analysis of the images. Fig. 4a shows the image of one slice. The full stack of images (Fig. 4b) was first smoothened using a median filter, with a neighborhood of 6, using 5 iterations. Watershed segmentation was used next to distinguish and separate pores from the
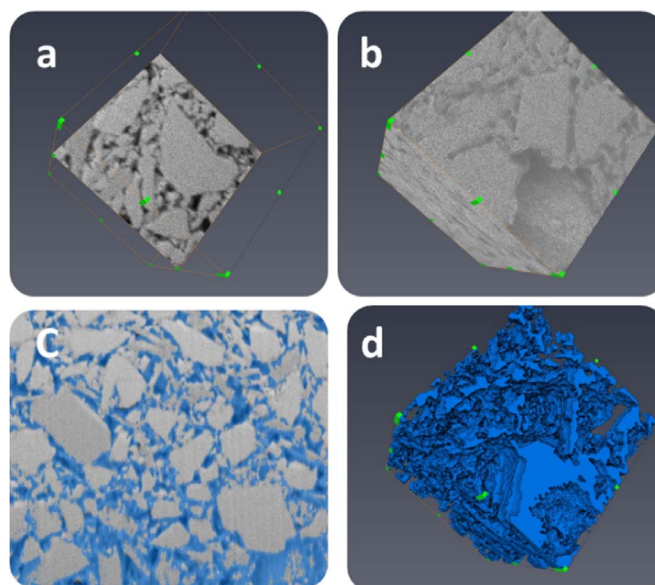
solid structures (Fig. 4c). The threshold values for the solid phase were manually chosen by comparing real gray scale images with the segmented images. With the above segmentations, the 3D structure of the coating layer could be reassembled and visualized (Fig. 4d).

The Avizo label analysis module was used to calculate the volume of pores. This module performs a connectivity analysis of individual pores within the entire 3D volume. The calculated volumes were needed for the porosity calculations.

2.4. Pore scale contact angle

The contact angle, ψ, is one of the key parameters affecting fluid retention and movement. We note that the contact angle is different from the spreading angle, which is measured as the edge angle of a droplet lying on the paper surface. This angle decreases with time as the liquid penetrates into the substrate. The contact angle, on the other hand, is the angle that a fluid-fluid interface inside a capillary forms with the pore wall. Under static isothermal conditions, this is a constant property of the two fluids involved (air, water) and the solid. Practical limitations of the microscopy techniques make it difficult to measure the real contact angle of liquids inside a single pore (in our case having an average diameter of only about 180 nm). Nevertheless, various approaches have been employed to estimate the contact angle. Here we used an average value of 45° for the contact angle based on studies by Järnström et al. (2010).

2.5. Determination of hydraulic properties

Upon arrival of an ink droplet, fluid will start moving into the pore network of dry paper (initially filled completely with air). Replacement of air by the invading liquid during ink setting constitutes an imbibition (wetting) process. Full characterization and simulations of the imbibition process requires information about several key parameters such as the pore size distribution, the porosity, and the capillary pressure – saturation (P_c-S) curve (Song et al., 2016). The 3D pore structure of the coating layer was used as input of the GeoDict software (Math2Market, Kaiserslautern, Germany) to obtain estimates of the capillary pressure (P_c-S) and relative permeability (K_r-S) curves. GeoDict uses for this purpose the pore morphology method (Schulz et al., 2015), which calculates the stationary distributions of the wetting and non-wetting phases at a given capillary pressure (Fig. 5). This approach neglects
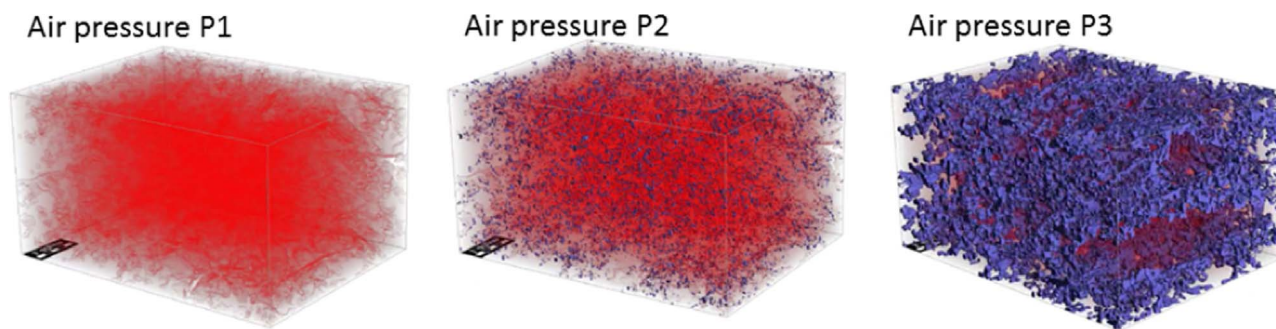
Fig. 5. Images of the sample at three different air pressures during imbibition, with pressures P1 > P2 > P3. The red and blue colors represent air and water filled pores, respectively. (For interpretation of the references to color in this figure legend, the reader is referred to the web version of this article.)

gravity effects and requires a known value for the contact angle.

For any given capillary pressure, a critical pore size is calculated based on the Young- Laplace equation:

$$r = \frac{2\sigma}{P_c} \cos \psi \tag{1}$$

where σ is surface tension, ψ the contact angle, and P_c the capillary pressure. For imbibition, initially, all pores are filled by the non-wetting phase. We then search for all pores whose size is equal to or smaller than the critical pore size r_c and are connected to the wetting phase reservoir. All those pores are assumed to become filled with the wetting phase (Hilpert et al., 2001). For drainage, all pores are at first filled with the wetting phase and we search for all pores whose size is equal to or larger than the critical pore size r_c and are connected to the nonwetting phase reservoir. All those pores are assumed to become invaded by the non-wetting phase. At the end of drainage process, a certain part of the wetting phase may remain trapped in some pores, which leads to irreducible wetting saturation. Similarly, at the end of an imbibition process, the non-wetting phase may remain trapped in some pores, thus producing residual non-wetting saturation.

The relative permeability under imbibition was determined based on the distribution of phases obtained with the pore morphology method during imbibition. Thus, in order to calculate the relative permeability at a given saturation, the distribution of the phases (wetting and non-wetting) were determined. A pressure gradient was subsequently imposed on each phase and flow was simulated by solving Stokes equation. Flow of each phase was assumed to be independent of flow of the other phase (i.e., transfer of momentum along the phase interfaces was not considered). The permeability of each phase was then determined by substituting the pressure gradient and total flow rate in Darcy's law. We refer to several previous studies for details (Schulz et al., 2014); (Hilpert et al., 2001); (Cheng et al., 2013).

3. Results

3.1. Pore size distribution

Properties of the pore structure of the coating layer are listed in Table 1. The total porosity of the sample was found to be 0.34 which is in good agreement with independent mercury porosity measurements as well as previous literature (Gane et al., 1996). The pore size distribution showing the probability of the various pore sizes is given in Fig. 6. The average pore size was 180 nm, which means that the
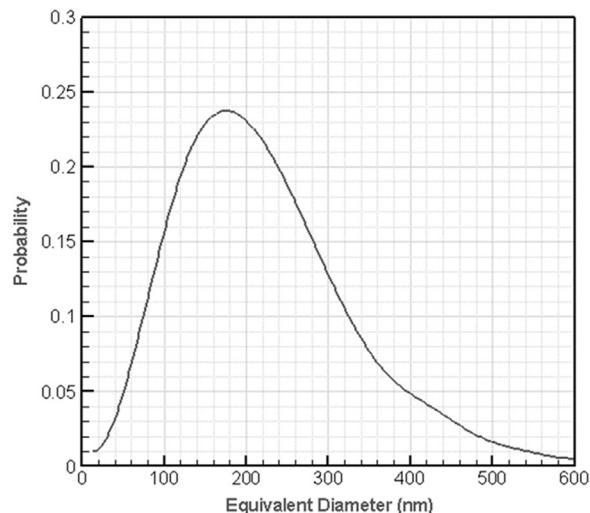

Fig. 6. The pore size distribution of the paper coating.

coating has a high capillary suction.

3.2. Hydraulic properties of the coating

3.2.1. Representative elementary volume (REV)

An important issue to be considered before performing pore-scale simulations is the minimum domain size that provides statistically meaningful parameter values. Calculated hydraulic properties for such a domain are then relatively insensitive to the pore network size. Such a representative network size will be considered as the REV of the porous medium being modeled. The REV size in our study was determined by calculating values of the porosity and permeability for different domain sizes, and plotting the results versus the domain dimension. Our results in Fig. 7 show that the porosity and permeability increased with domain size up to a domain of about 60 μm^3, above which they remained essentially constant at values of 0.34 and 0.1 mDarcy, respectively. For domains larger than 60 μm^3, the porosity and permeability changed less than 3%. Based on these results, we used a domain size of 60 μm^3 as the REV in our study.

3.2.2. Capillary pressure- saturation (P_c-S) and relative permeability (K_r-S) curves

The capillary pressure curves associated with drainage and imbibi-

Table 1
Pore network parameters of the coating.

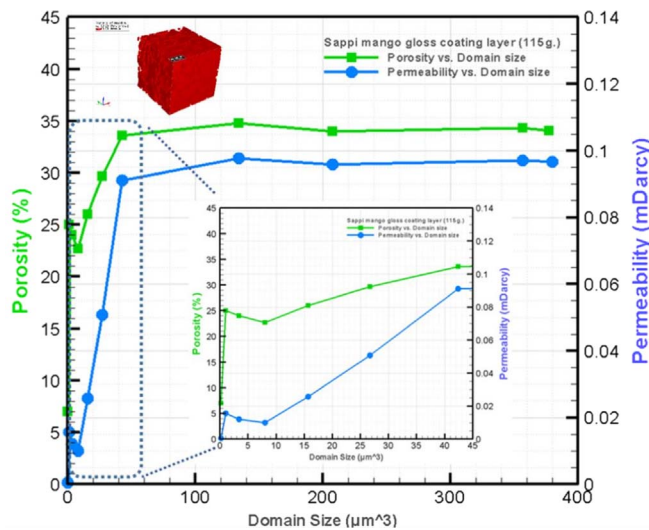| Total surface area (μm^2)	Ave. pore eq. diameter (nm)	Total no. pores	Porosity			Pore volume (nm^3)		
1273	180	31587	Porosity 0.34	Open porosity 0.339	Closed porosity 0.001	Min. 1213	Max. 113e6	Ave. 118e4

Fig. 7. Plots of calculated porosity and permeability values for different domain sizes of the coating.
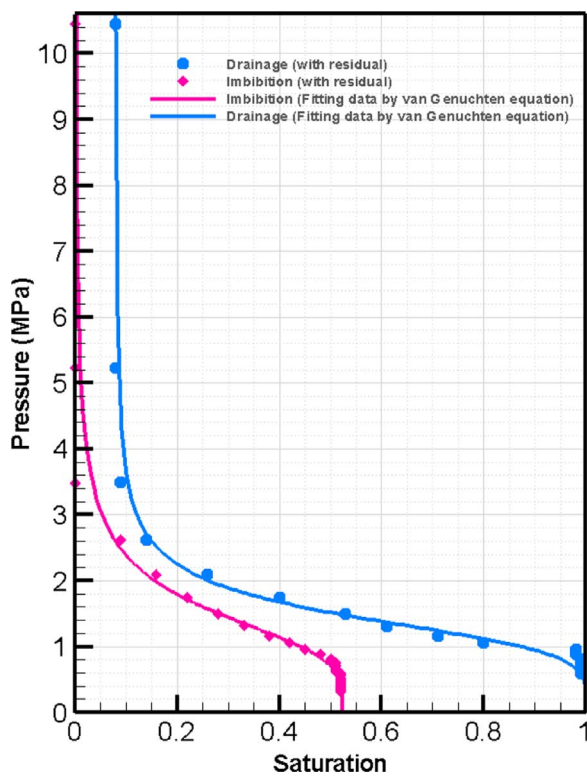

Fig. 8. Estimated P_c-S curves of the coating of a paper sample. Symbols represent simulation results obtained with the pore morphology method, while solid lines are based on the fitted van Genuchten-Mualem equation.

tion obtained with the software GeoDict, are shown in Fig. 8. The plots show that the air entry suction during both drainage and imbibition was very high (about 1 MPa or 10 bar). This feature of the coating is very favorable for printing purposes. Having a high capillary suction means that the ink (or droplet) will invade the coating as soon as the droplet touches the surface of the coating layer. The macroscopic (bulk) hydraulic parameters for fluid movement in a variably-saturated coating layer can be determined by fitting an empirical equation to the simulated P_c-S data. While several equations for the P_c–S curve can be used for this purpose (e.g., Leij et al., 1997), in this study we use the van Genuchten-Mualem model (van Genuchten, 1980), which is often used in numerical studies of fluid flow in variably-saturated media. The

Table 2
Values of the van Genuchten parameters of the Pc-S curves in Fig. 8.

	n	α (kPa^{-1})	S_r	S_{ir}
Primary Imbibition	3.96	0.712	0.476	0.000
Primary Drainage	5.00	0.731	0.00	0.082

capillary pressure- saturation relationship is then given by

$$S_e(P_c) = [1 + (\alpha P_c)^n]^{-m}, \quad S_e = \frac{S_w(P_c) - S_{ir} - S_r}{1 - S_{ir} - S_r} \tag{2}$$

where S_e, S_r, S_{ir}, and S_w, are effective saturation, air residual saturation, irreversible wetting phase saturation, and wetting phase saturation, respectively, P_c is the capillary pressure, α and n are empirical shape parameters reflecting the average pore size and width of the pore-size distribution, respectively, and $m=1-1/n$. The parameter α is closely related to the inverse of the air-entry capillary pressure of the medium (Luckner et al., 1989). The fitting parameters for the primary imbibition and drainage curves are shown in Table 2; they are in good agreement with the hydraulic parameters reported for similar porous materials having relatively narrow pore-size distribution (Carsel and Parrish, 1988; Ghanbarian-Alavijeh et al., 2010).

As explained above, relative permeability at different saturations imbibition was calculated using phases distribution determined by pore morphology method. Results for the primary imbibition are shown in Fig. 9 as symbols. Values are given up to a saturation of 0.534, which was the largest saturation value reached with the Pc- S imbibition curve.

The relative permeability can be also determined based on Eq. (2). On the basis of the van Genuchten- Mualem model (van Genuchten, 1980), the relative permeability of the wetting phase (k_{rw}) is given by

$$k_{rw} = s_e^l \{1 - [1 - s_e^m]^{1/m}\}^2 \tag{3}$$

where l is a pore connectivity parameter, generally set equal to 0.5 following the early work by Mualem (1976) and van Genuchten (1980). Sometimes, however, its value is fitted to experimental data in order to have more flexibility in describing observed relative permeability data ((Luckner et al., 1989; Leij et al., 1997)). Here we kept the original value of 0.5 for l.

The calculated relative permeability curve for primary imbibition is shown in Fig. 9 as a solid line. Good agreement was obtained between the relative permeability values calculated using the pore morphology method and the van Genuchten-Mualem equation as based on the primary imbibitioncurve. Eq. (3) provided only slightly higher values of
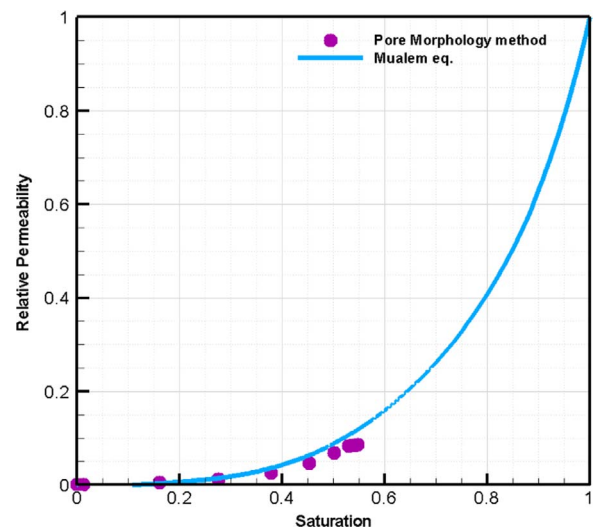

Fig. 9. Relative permeability curves for the wetting phase.

the calculated data points. Moreover, differences between the calculated primary drainage and imbibition curves using Eq. (3) with the parameter values in Table 1 were found to be negligible, indicating that hysteresis between the primary drainage and imbibition curves can be ignored when plotting results as a function of saturation. This is very much in agreement with many previous studies of flow in variably-saturated porous media.

4. Conclusions

The standard focused ion beam scanning electron microscope (FIB-SEM) used in our study was found to be a very effective technique for visualizing the three-dimensional morphology of coating layers of paper. In combination with image analysis methods, the technique was used to extract a 3D pore network of the coating layer. By analyzing segmented images, the pore size distribution and porosity of the coating could be determined. The minimum domain size for obtaining statistically meaningful values for porosity and permeability (REV) was found to be 60 μm^3. Capillary pressure – saturation (P_c- S) and relative permeability (K_r-S) values for the coating were obtained using the GeoDict software, based on the pore morphology method. By fitting the van Genuchten-Mualem equation to the Pc- S data, required parameters for calculation of the relative permeability were determined. The resulting hydraulic functions and its parameters provide a macroscopic characterization of the coating layer. These function can be used in continuum models for simulating ink penetration and spreading inside the coating layers of paper.

References

Alam, P., Byholm, T., Kniivilä, J., Sinervo, L., Toivakka, M., 2009. Calculating the permeability of model paper coating structures comprising incongruent particle shapes and sizes. Microporous and Mesoporous Materials 117 (3), 685–688. http://dx.doi.org/10.1016/j.micromeso.2008.08.002.

Bosanquet, C.H., 1923. LV. On the flow of liquids into capillary tubes. The London, Edinburgh, and Dublin Philosophical Magazine and Journal of Science 45 (267), 525–531. http://dx.doi.org/10.1080/14786442308634144.

Carsel, R.F., Parrish, R.S., 1988. Developing joint probability distributions of soil water retention characteristics. Water Resour. Res. 24 (5), 755–769.

L. Cheng R. Kirsch A. Wiegmann P.C. Gervais N. Bardin-Monnier D. Thomas PleatLab. A pleat scale simulation environment for filtration simulation In Proceedings of the FILTECH 2013 Conference

Dalton, J.S., Preston, J.S., Heard, P.J., Allen, G.C., Elton, N.J., Husband, J.C., 2002. Investigation into the distribution of ink components throughout printed coated paper: Part 2: Utilising XPS and SIMS.. Colloids Surfaces A : Physicochem and Engneering Aspects 205 (3), 199–213.

Desie, G., Deroover, G., De Voeght, F., Soucemarianadin, A., 2004. Printing of dye and pigment-based aqueous inks onto porous substrates. J. Imaging Sci. Technol. 48 (5), 389–397.

Gane, P.A., Salo, M., Kettle, J.P., Ridgway, C.J., 2009. Comparison of Young-Laplace pore size and microscopic void area distributions in topologically similar structures: a new method for characterising connectivity in pigmented coatings. J. Mater. Sci. 44 (2), 422–432.

Ghanbarian-Alavijeh, B., Liaghat, A., Huang, G.-H., van Genuchten, M. Th., 2010. Estimation of the van Genuchten soil water retention properties from soil textural data. Pedosphere 20 (4), 456–465.

Girard, F., Attané, P., Morin, V., 2006. A new analytical model for impact and spreading of one drop: Application to inkjet printing. Tappi J. 5 (12), 24–32.

Heard, P.J., Preston, J.S., Parsons, D.J., Cox, J., Allen, G.C., 2004. Visualisation of the distribution of ink components in printed coated paper using focused ion beam techniques. Colloids Surfaces A Physicochem. Eng. Asp. 244 (1), 67–71.

Markus, H., Miller, C.T., 2001. Pore-morphology-based simulation of drainage in totally wetting porous media. Advances in Water Resources 24 (3), 243–255.

Järnström, J., Väisänen, M., Lehto, R., Jäsberg, A., Timonen, J., Peltonen, J., 2010. Effect of latex on surface structure and wetting of pigment coatings. Colloids and Surfaces A : Physicochemical Engineering Aspects 353 (2), 104–116.

Karwacki, L., de Winter, D.A., Aramburo, L.R., Lebbink, M.N., Post, J.A., Drury, M.R., Weckhuysen, B.M., 2011. Architecture-dependent distribution of mesopores in steamed zeolite crystals as visualized by FIB-SEM tomography. Angewandte Chemie International Edition 50 (6), 1294–1298.

Kettle, J., Lamminmäki, T., Gane, P., 2010. A review of modified surfaces for high speed inkjet coating. Surface and Coatings Technology 204 (12), 2103–2109.

Lamminmäki, T.T., Kettle, J.P., Puukko, P.J.T., Ridgway, C.J., Gane, P.A.C., 2012. Short timescale inkjet ink component diffusion: an active part of the absorption mechanism into inkjet coatings. Journal of Colloid Interface Science 365 (1), 222–235.

Leij, F.J., Russell, W.B., Lesch, S.M., 1997. Closed-form expressions for water retention and conductivity. Ground Water 35 (5), 848–858.

Luckner, L., van Genuchten, M.T., Nielsen, D.R., 1989. A consistent set of parametric models for the two-phase flow of immiscible fluids in the subsurface. Water Resources Research 25 (10), 2187–2193.

Malla, P.B., Devisetti, S., 2005. Novel kaolin pigment for high solids ink jet coating. Paper Technology 46 (8), 17–27.

Matilainen, K., Hämäläinen, T., Savolainen, A., Sipiläinen-Malm, T., Peltonen, J., Erho, T., Smolander, M., 2012. Performance and penetration of laccase and ABTS inks on various printing substrates. Colloids and Surfaces B: Biointerfaces 90, 119–128.

Gane, P.A., Kettle, J.P., Matthews, G.P., Ridgway, C.J., Void space structure of compressible polymer spheres and consolidated calcium carbonate paper-coating formulations. *Industrial & engineering chemistry research* 35(5), 1996, 1753-1764.

Ridgway, C.J., Gane, P.A.C., 2002. Controlling the absorption dynamic of water-based ink into porous pigmented coating structures to enhance print performance. Nordic Pulp and Paper Research Journal 17 (2), 119–129.

Ridgway, C.J., Gane, P.A.C., Schoelkopf, J., 2002. Effect of capillary element aspect ratio on the dynamic imbibition within porous networks. Journal of Colloid Interface Science 252, 373–382.

Schoelkopf, J., Gane, P.A., Ridgway, C.J., Matthews, G.P., 2002. Practical observation of deviation from Lucas–Washburn scaling in porous media. Colloids Surfaces A: Physicochemical and Engineering Aspects 206 (1), 445–454.

Schulz, V.P., Wargo, E.A., Kumbur, E.C., 2015. Pore-morphology-based simulation of drainage in porous media featuring a locally variable contact angle. Transport in Porous Media 107 (1), 13–25.

Song, Y., Davy, C.A., Bertier, P., Troadec, D., 2016. Understanding fluid transport through claystones from their 3D nanoscopic pore network. Microporous Mesoporous Mater. 228, 64–85.

van Genuchten, M. Th. "A closed-form equation for predicting the hydraulic conductivity of unsaturated soils." *Soil science society of America journal* 44 (5), 1980, 892-898.

Vikman, K., Vuorinen, T., 2004. Water Fastness of Ink Jet Prints on Modified Conventional Coatings, vol. 48. pp. 138–147